JOURNAL OF COMPUTATIONAL PHYSICS 84, 461–473 (1989)

An Improved Upwind Scheme for the Euler Equations

SHEN-MIN LIANG AND JYH-JANG CHAN

Institute of Aeronautics and Astronautics, National Cheng Kung University, Tainan, Taiwan, 70101 Republic of China

Received October 26, 1987; January 18, 1989

An implicit upwind scheme of almost second-order accuracy is developed for solving the Euler equations in a conservative form. The scheme is obtained by modifying the Coakley dissipation function and introducing a smooth transition function at the sonic point. The smooth transition function was introduced to avoid the sonic-line glitch due to the eigenvalue switching. Since upwind differencing is naturally dissipative, the stability of the present scheme is enhanced. Numerical results demonstrate that the present scheme is as accurate as the TVD scheme (Yee, Warming, and Harten, *AIAA Paper* 83-1902, 1983) and as efficient as other upwind schemes (Coakley, *AIAA* 83–1958, 1983).

1. INTRODUCTION

In recent years many researchers have focused on the study of efficient high resolution schemes for hyperbolic systems of conservation laws [1–8]. Generally speaking, the schemes used for a hyperbolic system may be classified into three categories: (1) space centered schemes; (2) TVD schemes; (3) upwind schemes. The space centered schemes [9, 10] require an additional artificial viscosity for stable computation. The damping coefficient must be carefully tuned for different problems. The delicate TVD scheme, first introduced by Harten, is successful in generating oscillation-free solutions, but needs much longer CPU time due to more operations (or function evaluations) for each iteration. The upwind schemes [5, 6, 8] of flux vector splitting are based on characterstic theory and possess natural dissipation. The split-flux vectors of Steger and Warming [8] might produce a glitch near the sonic point due to eigenvalue switching. To smooth out the sonic-line glitch, Buning and Steger [11] introduced continuous split eigenvalues to replace discontinuous split eigenvalues. The modification in the split eigenvalues is equivalent to adding a dissipation term of fourth derivative [12]. Another approach to the eigenvalue switching problem has been proposed by van Leer [13].

In 1981 Huang [2] introduced an first-order upwind scheme which can capture a sharp shock front in the vicinity of the shock; but it also can generate a glitch (or kink) at the sonic point. In the Huang's scheme, the dissipation function is proportional to flux difference. The proportionality is a matrix with elements dependent on

0021-9991/89 $3.00

581/84/2-14

the eigenvectors and the sign of local eigenvalues. In 1983 Coakley [6] introduced a second-order upwind scheme which seems to produce an oscillation-free solution near the normal shock in 2-dimensional transonic airfoil calculations. However, it was found that the scheme could generate one point overshoot near the normal shock in quasi-1-dimensional problems. Our computational results indicate that the amplitude of the one point overshoot increases for stronger shocks or on finer grids.

In this paper, we use a variant form of the Coakley dissipation function and introduce a continuous transition function at the sonic point to avoid the sonic-line glitch. The resulting scheme is constructed in a finite-volume fashion and is second-order accurate except near the sonic point. Our numerical experiments indicate that the improved scheme produces a continuous solution across the sonic point and captures a sharp shock front. The scheme is as accurate as the TVD scheme of Yee, Warming, and Harten [1] and is as efficient as other upwind schemes [2].

2. Mathematical Notation

The numerical scheme is presented for 1-dimensional Euler equations and the flux–vector splitting is briefly reviewed in order to establish the necessary notation for the modified numerical scheme. Its extension to the two and three dimensions is straightforward.

The 1-dimensional Euler equations are

$$\partial_t U + \partial_x F = 0, \tag{1}$$

where

$$U = \begin{pmatrix} \rho \\ \rho u \\ \rho E \end{pmatrix}, \qquad F = \begin{pmatrix} \rho u \\ \rho u^2 + p \\ (\rho E + p)\, u \end{pmatrix} \tag{2}$$

are the conservative variables and the flux vectors. In Eq. (2), ρ is the density, u the velocity, $p = \rho c^2/\gamma$ the pressure, ρE the total energy, γ the ratio of specific heats, and c the speed of sound. The Jacobian matrix A, defined by $\partial F/\partial U$, can be diagonalized by a similarity transformation, L:

$$A = \frac{\partial F}{\partial U} = L^{-1} \Lambda L$$

where $\Lambda = \text{diag}(u, u + c, u - c)$ is formed by eigenvalues of A and L is the matrix composed of the corresponding left eigenvectors. Since F is a homogeneous function of degree one, thus $F = AU$. Steger and Warming split the flux vector based on the local eigenvalue.

$$\begin{aligned} F &= AU \\ &= (L^{-1}\Lambda L)\, U \\ &= [L^{-1}(\Lambda^+ + \Lambda^-)\, L]\, U \\ &= (A^+ + A^-)\, U \\ &= F^+ + F^-, \end{aligned}$$

where $\Lambda^{\pm} = \frac{1}{2}(\Lambda \pm |\Lambda|)$. Define a matrix $S = L^{-1}\,\mathrm{sgn}(\Lambda)\, L$. Then

$$SF = L^{-1}|\Lambda|\, W, \qquad W = LU.$$

Note that some elements are discontinuous in S at the sonic point, as shown below:

$$S = \begin{pmatrix} (1-\gamma)/2 & \gamma/c & (1-\gamma)/c^2 \\ 0 & 1 & 0 \\ c^2(\gamma^2-2\gamma-3)/4(\gamma-1) & c\gamma(3-\gamma)/2(\gamma-1) & (\gamma-1)/2 \end{pmatrix} \quad \text{for} \quad M<1,$$

$$S = \begin{pmatrix} (3-\gamma)/4 & \gamma/2c & (1-\gamma)/2c^2 \\ 0 & 1 & 0 \\ c^2(\gamma^2-2\gamma-3)/8(\gamma-1) & c\gamma(3-\gamma)/4(\gamma-1) & (1+\gamma)/4 \end{pmatrix} \quad \text{for} \quad M=1,$$

and

$$S = \begin{pmatrix} 1 & 0 & 0 \\ 0 & 1 & 0 \\ 0 & 0 & 1 \end{pmatrix} \quad \text{for} \quad M>1.$$

3. Numerical Method

Implicit Upwind-Differencing Algorithm

Using backward time-differencing, the basic implicit algorithm can be written in a delta form

$$(I + \Delta t\, \partial_x A)\, \Delta U = -\Delta t\, \partial_x F, \tag{3}$$

where $\Delta U = U(x, t+\Delta t) - U(x, t)$ is the delta variable and Δt is the time step.

The spatial derivative in the right-hand side of Eq. (3) is approximated, in a finite-volume form, by

$$\partial_x F = \frac{(\hat{F}_{i+1/2} - \hat{F}_{i-1/2})}{\Delta x}, \tag{4}$$

where Δx is the grid spacing and $\hat{F}_{i+1/2}$ is the numerical flux vector defined at the cell interface between grid points i and $i+1$. Regardless of the form of $\hat{F}_{i+1/2}$, Eq. (4) represents a conservative differencing. The numerical flux vector can be defined in terms of U_{i-1}, U_i, U_{i+1}, U_{i+2} as

$$\hat{F}_{i+1/2} = \tfrac{1}{2}(F_i + F_{i+1} - D_{i+1/2}). \tag{5}$$

By using the characteristic variable, W, Coakley constructed the following expression for the dissipation function, D:

$$D_{i+1/2} = L^{-1}_{i+1/2}(|\Lambda|_{i+1/2}\,\Delta W_{i+1/2} + \Lambda^{-}_{i+1/2}\,\Delta W_{i+3/2} - \Lambda^{+}_{i+1/2}\,\Delta W_{i-1/2}), \tag{6}$$

where

$$\Delta W_{i+1/2} = L_{i+1/2}(U_{i+1} - U_i).$$

Note that D is of second order. It was found that the Coakley dissipation function can produce an overshoot near the shock and the overshoot is worse for a stronger shock. In Huang's first-order scheme, the dissipation function (6) used is

$$D_{i+1/2} = S_{i+1/2}\,\Delta F_{i+1/2},$$

which can generate an oscillation-free solution. Since $S\,\Delta F = L^{-1}|\Lambda|\,\Delta W$, the Coakley dissipation function is rewritten as

$$D_{i+1/2} = S_{i+1/2}\,\Delta F_{i+1/2} + L^{-1}_{i+1/2}(\Lambda^{-}_{i+1/2}\,\Delta W_{i+3/2} - \Lambda^{+}_{i+1/2}\,\Delta W_{i-1/2}). \tag{7}$$

The modified dissipation function is able to capture a sharp shock front, but also generates a sonic-line glitch which is caused by the eigenvalue switching. A similar situation has been reported in Ref. [8]. Since there is a discontinuity in S when the eigenvalue changes sign, the dissipation function (7) is further modified by introducing a continuous transition function at the sonic point. The particular form of this transition function used in this paper is

$$\mu(M) = \tanh[k(M-1)^3], \tag{8}$$

where M is the Mach number and k is a parameter to control the width of the transition region. Other functions such as in [1] failed in the present scheme. The introduction of the transition function degrades the scheme accuracy from second order to first order. Since the value of the transition function must be -1 upstream of the sonic point and $+1$ downstream of the sonic point and $\tanh(x)$ is almost unity when $x = 3$, the transition region is determined by choosing a value of k. For example, if $k = 400$, the transition occurs from $M = 0.804$ to $M = 1.196$. The curve of μ is shown in Fig. 1. The width of the transition region can be narrowed down

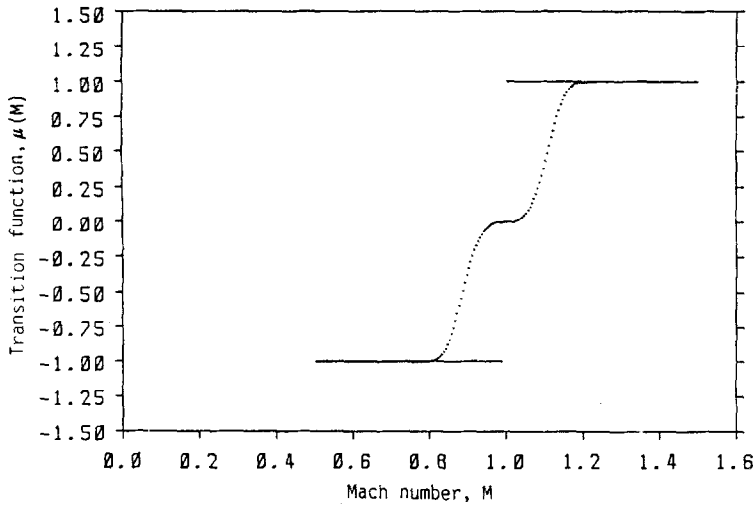

FIG. 1. The transition function: $\mu(M) = \tanh(400 \times (M-1)^3)$.

if the grid point is dense at the sonic point. The matrix S with the transition function in the neighborhood of the sonic point becomes

$$S = \begin{pmatrix} (3-\gamma+(\gamma+1)\,\mu)/4 & \gamma(1-\mu)/2c & (\gamma-1)(\mu-1)/2c^2 \\ 0 & 1 & 0 \\ c^2(\gamma^2-2\gamma-3)(1-\mu)/8(\gamma-1) & c\gamma(3-\gamma)(1-\mu)/4(\gamma-1) & (1+\gamma+(3-\gamma)\,\mu)/4 \end{pmatrix}.$$

It is clear that every element in S is continuous across the sonic point. Hence the new dissipation function does not produce any kink at the sonic point.

The method of Roe's averaging [5] is used for computing $S_{i+1/2}$, $L_{i+1/2}$, etc., in terms of U_i, and U_{i+1} on the interface of control volumes. This leads to

$$a = \left(\frac{\rho_i + 1}{\rho_i}\right)^{1/2}$$

$$u_{i+1/2} = \frac{a u_{i+1} + u_i}{1+a}$$

$$c^2_{i+1/2} = (\gamma-1)\left(\frac{aH_{i+1} + H_i}{1+a} - \frac{u^2_{i+1/2}}{2}\right),$$

where $H = E + p/\rho$.

Finally, the upwind-difference scheme is used for the $\partial_x A$ in Eq. (3). It becomes

$$L^{-1}\left[I + \frac{\Delta t}{\Delta x}(\Lambda^+\delta^- + \Lambda^-\delta^+)\right] L\,\Delta U = -\frac{\Delta t}{\Delta x}(\hat{F}_{i+1/2} - \hat{F}_{i-1/2}),$$

where δ^+ and δ^- denote the forward- and backward-difference operators, respectively. Advantages of this algorithm are that (i) is substantially reduces computing time compared with the more exact block-tridiagonal form and (ii) the upwind differencing is naturally dissipative and enhances the stability of the overall algorithm.

4. Results and Discussion of Test Cases

First, we consider a quasi-1-dimensional supersonic flow through a divergent nozzle whose cross-section area is

$$A(x) = 1.398 + 0.347 \tanh(0.8x - 4), \qquad 0 \leqslant x \leqslant 10.$$

For a supersonic inflow, the flow variables (ρ, u, E) are specified. At the outlet, pressure is prescribed for a subsonic outflow. For flow variables not specified at the outlet, the characteristic is used to update their values at every iteration. The initial condition for interior points is approximated by using linear interpolation from the exact steady-state boundary-values.

The total number of grid points for all test cases is 60 unless otherwise specified. The grid points are uniformly distributed. All the calculations were performed on a VAX-8600 computer. The steady-state solutions are achieved when the residual measured by root-mean-square error in density is less than 5×10^{-7}. The Courant number, CFL, is chosen to be 10. The parameter k is chosen to be 1600. However, several values were tried and it was found that the results were very insentitive to the choice of the k value.

To see the accuracy of the present scheme, computed results are compared with the exact solutions and the results obtained by the Coakley scheme. Figures 2a and b show the pressure distributions for a supersonic divergent nozzle with the inflow Mach number, $M_{\text{in}} = 1.1$, and the back pressure, $p_b/p_t = 0.7$ and 0.8, where p_t denotes the inflow total pressure. The present method produces better resolutions than Coakley's, because no oscillations are generated in the vicinity of the shock. The convergent histories for these two cases are shown in Figs. 3a and b. It is apparent that the convergent rate of the present scheme is as fast as the Coakley scheme. In these two cases, there is no sonic point. Hence the transition function, μ, is not needed. To see the effect of the transition function we test the second case.

The second example is a subsonic flow through a convergent–divergent nozzle whose cross-section area is

$$A(x) = \begin{cases} 1 + 0.02(5 - x)^2, & 0 \leqslant x \leqslant 5; \\ 1 + 0.06(x - 5)^2, & 5 \leqslant x \leqslant 10. \end{cases}$$

For a subsonic inflow, two flow variables are specified at the inlet. We specify $\rho = \rho_0$ and $E = E_0$. For the convergent–divergent nozzle, the sonic point occurs at

the throat. This example can be used to test whether the scheme needs a smooth transition at the sonic point or not. Figure 4 shows that a glitch is produced near the sonic point if a smooth transition function is not introduced in expression (7). After the introduction of the smooth transition function (8), the present scheme produces an accurate solution without oscillations near the shock and the sonic-point glitch. Figure 5 shows the pressure distribution for the convergent–divergent

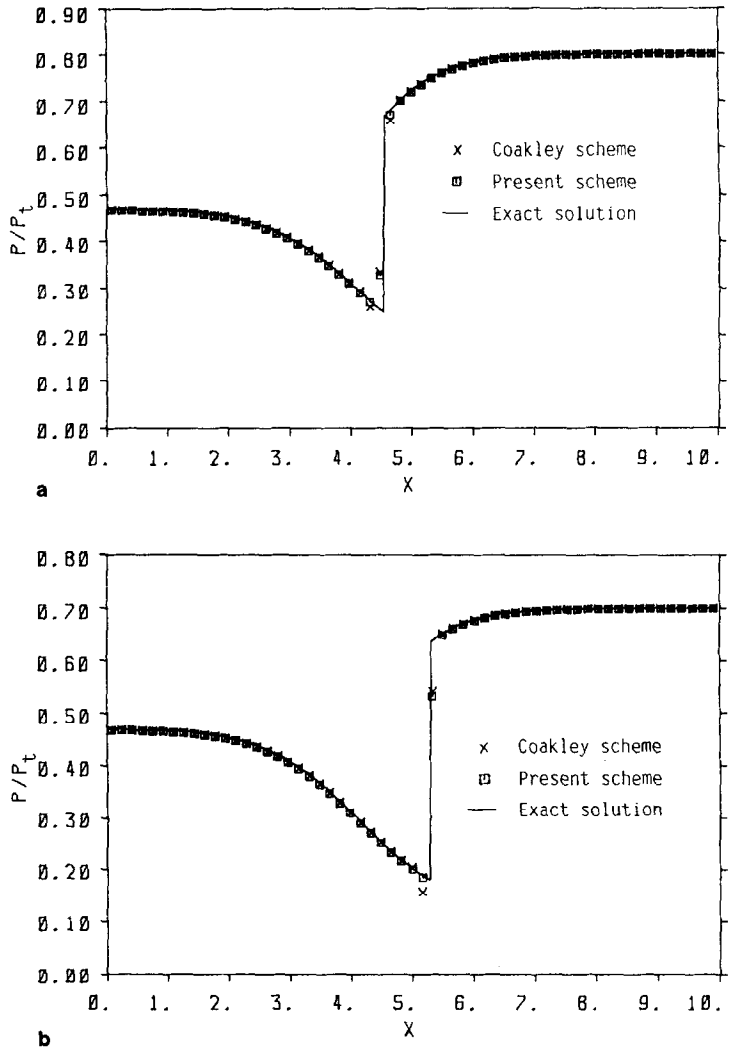

FIG. 2. (a) Comparison of pressure distribution with exact solution for a divergent nozzle with $p_b/p_t = 0.8$. (b) Comparison of pressure distributions with exact solution for a divergent nozzle with $p_b/p_t = 0.7$.

nozzle with the subsonic inflow, $M_{in} = 0.2395$, and the back pressure $p_b/p_t = 0.80$, by using the present scheme. The result is in good agreement with the exact solution. However, the present scheme needs more iterations for convergence. In this case, the present scheme needs 173 iterations, but the Coakley scheme needs 158 iterations. Normally, if the grid points are increased, the numerical solution would be closer to the exact solution. Figure 6 shows the refined solutions obtained by the present scheme and the Coakley scheme on a finer grid with 100 points.

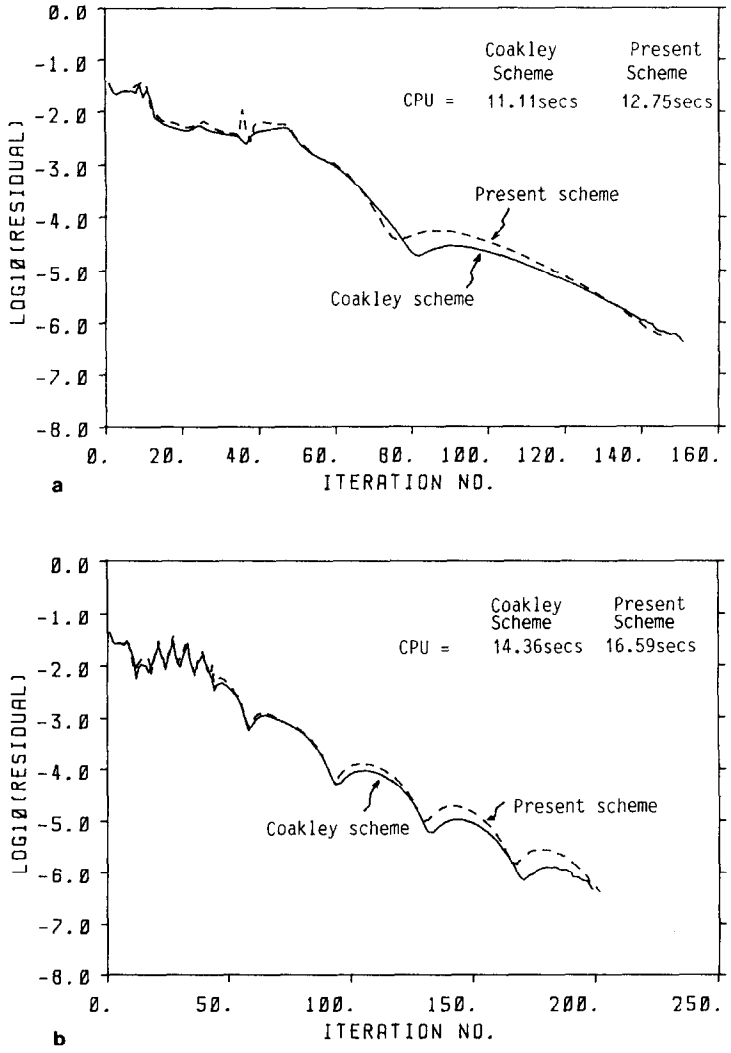

FIG. 3. (a) Comparison of convergent histories for different schemes, $p_b/p_t = 0.7$. (b) Comparison of convergent histories for different schemes, $p_b/p_t = 0.8$.

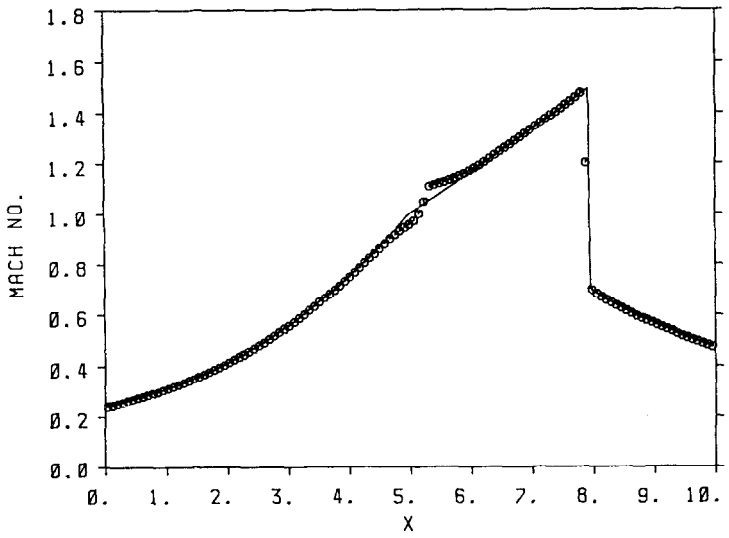

FIG. 4. Mach number distribution for a convergent–divergent nozzle, when smooth transition function is not introduced in Eq. (8).

Since the amplitude of the 1-point overshoot generated by the Coakley scheme increases, the results indicate that the present scheme can resolve the shock by grid refinement, but the Coakley scheme cannot. The present scheme takes approximately one-third times longer than the Coakley scheme.

The present result is also compared with that obtained by the implicit upwind

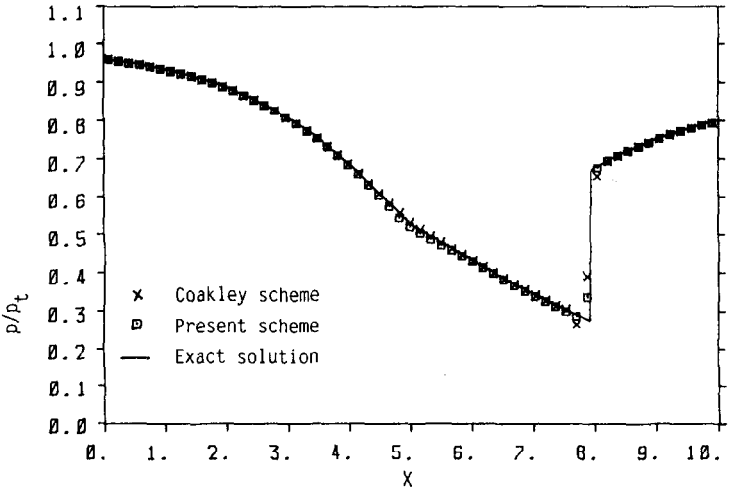

FIG. 5. Comparison of pressure distributions with exact solution for a convergent–divergent nozzle, $p_b/p_t = 0.8$.

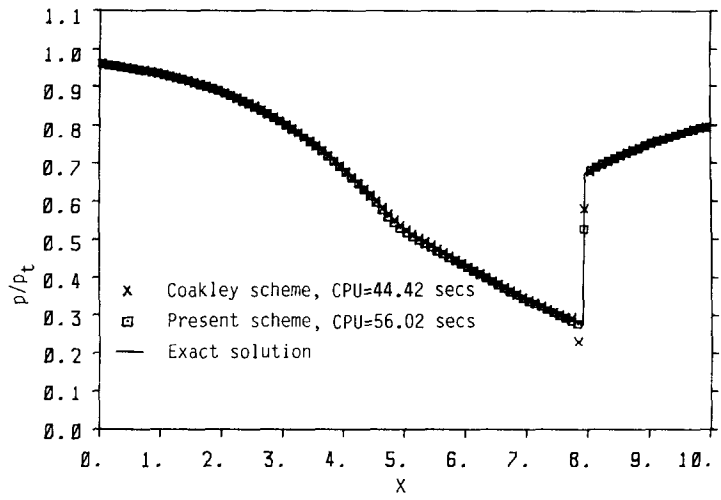

FIG. 6. Comparison of pressure distributions with exact solution after grid refinement for a convergent–divergent nozzle, $p_b/p_t = 0.8$.

second-order TVD scheme of Yee *et al.* Figure 7 shows the comparison of the computed results with the exact solution. Because the TVD scheme is written in a finite-difference fashion, the grid points used for the TVD scheme do not coincide with those used for the present scheme. It is hard to judge from this comparison which result is better, nevertheless, it indicates that the present result is as accurate as the TVD result. In this case the residual is set to 10^{-5}, because the TVD scheme cannot

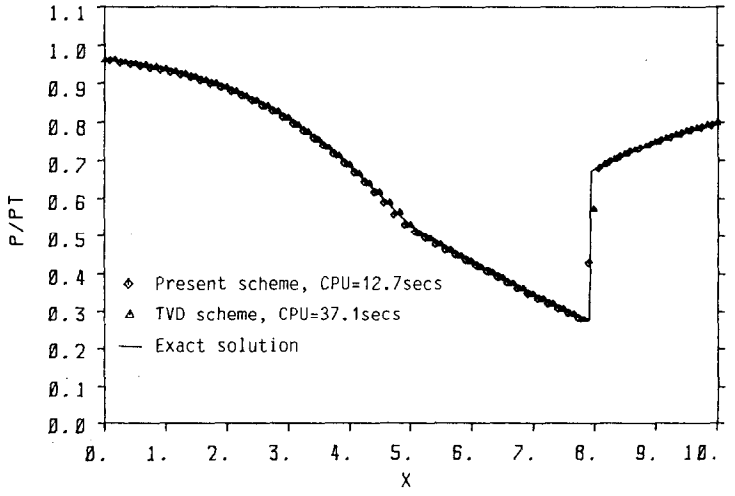

FIG. 7. Comparison of pressure distributions with the exact solution for a convergent–divergent nozzle with $p_b/p_t = 0.8$, using different schemes.

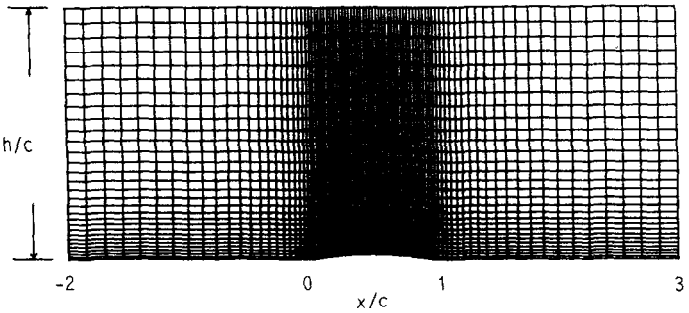

FIG. 8. Computational grid for transonic flow over a bump in a channel, $t/c = 4.2\%$, $h/c = 2$, grid: 85×30.

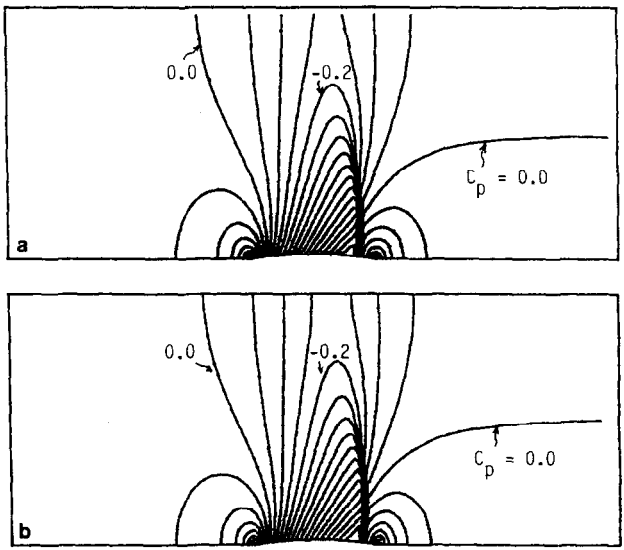

FIG. 9. Pressure contours for transonic channel flow, $M_\infty = 0.85$, $t/c = 4.3\%$, $\Delta C_p = 0.05$.

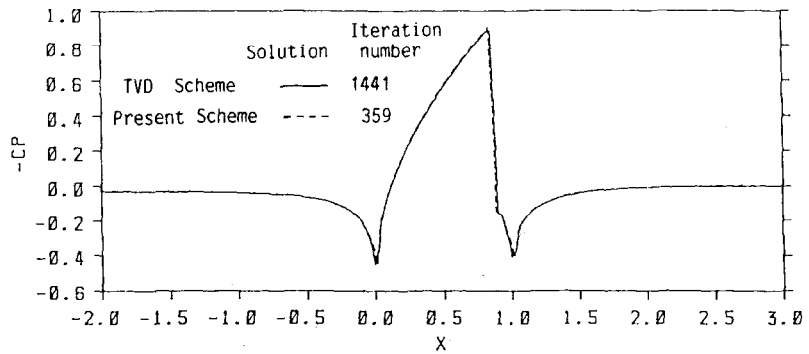

FIG. 10. Comparison of pressure distributions along the lower wall for transonic channel flow, $M_\infty = 0.85$, $t/c = 4.2\%$.

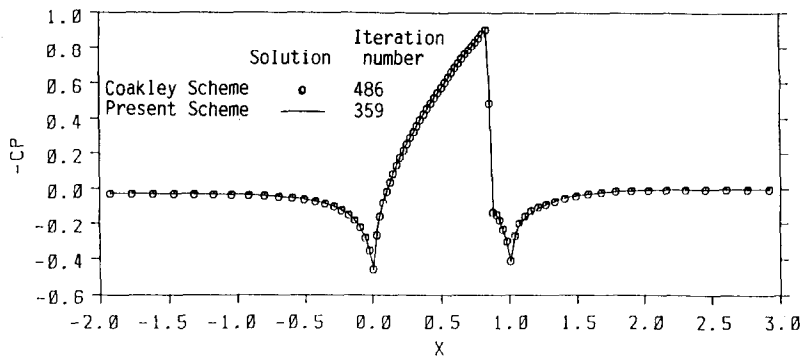

FIG. 11. Comparison of pressure distributions along the lower wall for transonic channel flow, $M_\infty = 0.85$, $t/c = 4.2\%$.

reach the previous convergence criterion. The convergent rate of the present scheme is three times faster than the TVD scheme.

The last example is a transonic flow over a bump in a channel. The thickness ratio is 4.2% and the freestream Mach number is 0.85. The inlet and outlet boundary conditions are similar to the first two examples. At the solid boundary, the tangency condition is used. In this case, it was found that the smooth transition function is not important. Figure 8 shows the grid system used. The grid points are clustered near the bump. Figures 9a and b are the pressure contours obtained by the present and TVD schemes, respectively. Both contours in Fig. 9 are very similar. A close look at the pressure distributions along the lower wall, as shown in Fig. 10, indicate that the present result is as accurate as the TVD result, with only one-third the number of iterations needed for the TVD scheme. Figure 11 presents the comparison of the present result with the Coakley result. Since the normal shock is not strong, the Coakley result is as accurate as the present result, but needs a larger number of iterations.

5. CONCLUSIONS

An improved implicit upwind scheme of almost second-order accuracy is developed for the calculation of 1- and 2-dimensional transonic flows. A continuous transition function is introduced in order to avoid the sonic-line glitch. However, the numerical experiments indicate that the smooth transition function is important only in the 1-dimensional problem and the present scheme is second order except near the sonic point. In two dimensions, the transition function is not needed, thus the present scheme is second-order accurate. Numerical results show that the present scheme is as accurate as the implicit TVD of Yee *et al.* and is as efficient as other upwind schemes.

ACKNOWLEDGMENTS

The authors thank Professor L. S. Yao, a visiting professor from Arizona State University, for reading and commenting on the manuscript.

REFERENCES

1. H. C. YEE, R. F. WARMING, AND A. HARTEN, Implicit total variation diminishing (TVD) schemes for steady-state calculations, *AIAA Paper* 83-1902, 1983.
2. T. J. COAKLEY, Implicit upwind methods for the compressible Navier–Stokes Equations, *AIAA Paper* 83-1958, 1983.
3. B. VAN LEER, Towards the ultimate conservative difference scheme II. Monotonicity and conservation combined in a second-order scheme, *J. Comput. Phys.* **14**, 361 (1974).
4. A. HARTEN, High resolution schemes for hyperbolic conservation laws, *J. Comput. Phys.* **49**, 357 (1983).
5. P. L. ROE, Approximate Riemann solvers, parameter vectors, and difference schemes, *J. Comput. Phys.* **43**, 357 (1981).
6. L. C. HUANG, Pseudo-unsteady difference schemes for one-dimensional fluid dynamics problems, *J. Comput. Phys.* **42**, 195 (1981).
7. S. OSHER AND S. CHAKRAVARTHY, High resolution schemes and the entropy condition, *SIAM J. Numer. Anal.* **21**, 955 (1984).
8. J. L. STEGER AND R. F. WARMING, Flux vector splitting of the inviscid gasdynamic equations with application to finite difference methods, *J. Comput. Phys.* **40**, 263 (1981).
9. R. M. BEAM AND R. F. WARMING, An implicit finite-difference algorithm for hyperbolic system in conservation-law form, *J. Comput. Phys.* **22**, 87 (1976).
10. A. JAMESON, W. SCHMIDT, AND E. TURKEL, Numerical solutions of the Euler equations by finite-volume methods using Runge–Kutta time stepping schemes, *AIAA Paper* 81-1259, 1981.
11. P. G. BUNING AND J. L. STEGER, Solution of the two-dimensional Euler equations with generalized coordinate transformation using flux vector splitting, *AIAA Paper* 82-0971, 1982.
12. P. G. BUNING, "Computation of Inviscid Transonic Flow Using Flux Vector Splitting in Generalizing Coordinates," Ph.D. dissertation, Stanford University, 1983.
13. B. VAN LEER, *Flux-Vector Splitting for the Euler Equations*, Lecture Notes in Physics, Vol. 170 (Springer-Verlag, New York/Berlin, 1982), p. 507.